Smart Structures and Systems, *Vol. 29, No. 6 (2022) 785-790*
https://doi.org/10.12989/sss.2022.29.6.785

Fault detection and classification of permanent magnet synchronous machine using signal injection

Inhwan Kim, Younghun Lee, Jaewook Oh and Namsu Kim*

Department of Mechanical engineering, Konkuk University, Seoul, Republic of Korea,
120 Neungdong-ro, Gwangjin-gu, Seoul, Republic of Korea

(*Received October 31, 2021, Revised February 1, 2022, Accepted April 26, 2022*)

Abstract. Condition monitoring of permanent magnet synchronous motors (PMSMs) and detecting faults such as eccentricity and demagnetization are essential for ensuring system reliability. Motor current signal analysis is the most commonly used precursor for detecting faults in the PMSM drive system. However, the current signature responds sensitively to the load and temperature of the motor, thereby making it difficult to monitor faults in real- applications. Therefore, in this study, a condition monitoring methodology that detects motor faults, including their classification with standstill conditions, is proposed. The objective is to detect and classify faults of PMSMs by using programmable inverter without additional sensors and systems for detection. Both DC and AC were applied through the d-axis of a three-phase motor, and the change in incremental inductance was investigated to detect and classify faults. Simulation with finite element analysis and experiments were performed on PMSMs in healthy conditions as well as with eccentricity and demagnetization faults. Based on the results obtained from experiments, the proposed method was confirmed to detect and classify types of faults, including their severity.

Keywords: fault detect; fault diagnosis; health management; inverter; magnetic saturation; permanent magnet synchronous motor; signal injection

1. Introduction

Recently, permanent magnet synchronous motors (PMSMs) have been spotlighted as eco-friendly traction systems that can replace internal combustion engines in various industrial fields owing to their high efficiency, output, and high torque at low speed (Bianchi and Jahns 2004, Liu *et al.* 2016, Chai *et al.* 2016).

PMSMs are classified into two categories depending on the position of the permanent magnet. The first is surface PMSMs (SPMSMs), in which permanent magnets (PMs) are attached to the surface of the rotor; they are affected by centrifugal force and have low durability. The second is interior PMSMs (IPMSMs) that have high durability and are suitable for high-speed rotation because the PMs are inserted inside the rotor. In addition, higher torque can be applied owing to the salient polarity. IPMSMs are mainly used in eco-friendly automobile markets and industries requiring high speed and torque (Soong and Erturgul 2002, Kiousmarsi *et al.* 2006, Fasil *et al.* 2016).

Major cases of PMSM failure include magnetic, mechanical, and electrical failures (Rajagopalan *et al*. 2006, Roux *et al.* 2007). Failures can be caused by manufacturing tolerances, harsh operating conditions, misalignment of shafts, and deterioration of components (Rosero *et al.* 2007). These failures adversely affect the reliability and safety of PMSMs. Numerous studies have been conducted to monitor the condition of machines to ensure high reliability and to prevent catastrophic failures. Frequently used motor condition monitoring methods such as motor current signal analysis (MCSA), motor voltage signal analysis (MVSA), and vibration signal analysis require additional sensors and systems for collecting and analyzing data (Nandi *et al*. 2001, Espinosa *et al*. 2001, Lee *et al*. 2011, Haddad *et al*. 2016). The characteristics in the frequency domain are investigated to detect faults, as shown in Eq. (1) where f_{fault} is the fault frequency, k is an integer, p is the number of pole pairs in the motor, and $f_{rotating}$ is the synchronous rotation frequency.

$$f_{fault} = (1 \pm k) \cdot p \cdot f_{rotating} \tag{1}$$

MCSA or MVSA is hard to implement in actual applications because inconsistent speeds and loads impact the performance of the diagnostic signal. (Rajagopalan *et al.* 2006). To overcome these issues, time-frequency analysis has been proposed, but it increases the required specification of the detection system (Roux *et al.* 2007). In addition, it becomes more difficult to classify faults and types because magnetic, mechanical, and electrical faults can all affect the fault frequency (f_{fault}) (Wu *et al.* 2007).

In this paper, a method to detect and classify faults of an IPMSM using a programmable inverter is proposed. With the implementation of the system, faults can be detected through algorithms using its embedded programs in the inverter without additional sensors or systems for analysis. For experimental validation of the proposed method, a Texas Instruments (TI) digital signal controller (TMS320F28335) was used in conjunction with MATLAB

*Corresponding author, Professor
E-mail: nkim7@konkuk.ac.kr

ISSN: 1738-1584 (Print), 1738-1991 (Online)

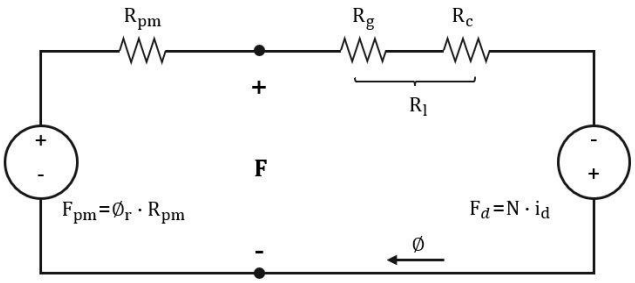

Fig. 1 Magnetic equivalent circuit representation of the *d*-axis flux path

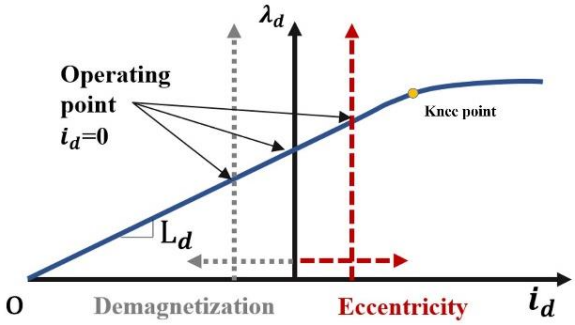

Fig. 2 *d*-axis flux linkage λ_d and current curve with eccentricity and demagnetization fault

Simulink. The inverter injects the optimized diagnostic signal (DC and AC current signal) into the motor when the motor is in a standstill condition. The differential inductance is calculated using the measured signal, and the types of faults were classified by comparing these values with reference values from the motor in the healthy state.

2. Analysis of *d*-axis flux linkage and inductance

2.1 Magnetic equivalent circuit of PMSM

Faults such as demagnetization and eccentricity cause deviation in motor inductance. Therefore, it is observed for the detection and classification of faults in this paper. The magnetic equivalent circuit is shown in Fig. 1 to present the effects of the PM, *d*-axis current, air gap, stator, and rotor core on the *d*-axis magnetic flux linkage. *F*, *R*, ∅, and *N* represent the magnetomotive force (MMF), reluctance, flux, and the number of turns of the motor winding, respectively. The subscripts *pm*, *g*, *c*, and *l* denote the PM, air gap, core, and load, respectively. Based on the magnetic equivalent circuit, it is confirmed that the flux increases around the stator on the side where the air gap decreases owing to the eccentricity. In addition, the flux around the stator decreases due to demagnetization. Both indicate that the changes in the magnetic properties of the PM and air gap impacts the flux around the stator as well as the *d*-axis flux.

The graph in Fig. 2 shows the inductance as a function of the d-axis current. The slope of this curve is the inductance, and the inductance change is the incremental inductance. The slope of this curve decreases as the operating point is close to the "knee point" as shown in Fig. 2. In the case of eccentricity fault, the operating point moves to the right which indicates that less current is required for magnetic saturation. In contrast, in the case of demagnetization fault, the operating point shifts to the left showing that more current is needed for saturation.

2.2 Differential inductance in d-axis

To maximize the sensitivity of detection, the *d*-axis of the IPMSM was aligned to the north pole of the PMs. Flux linkage in the *d*-axis (λ_d) is determined by the sum of the d-axis inductance (L_d) multiplied by the *d*-axis current (i_d) and the flux of the permanent magnet (λ_m), as shown in Eq. (2). The differential inductance of the *d*-axis can be derived through simple mathematical manipulation, as shown in Eq. (4).

Table 1 PMSM specification

Parameter	Detail
PMSM type	Interior PMSM
Winding type	Distributed double layer
Core material	30PNF1600
Magnet material	N42UH
Rated power (W)	400
Rated torque (Nm)	0.58
Rated speed (rpm)	6600
Rated voltage (V)	220
Pole number	4

$$\lambda_d = L_d i_d + \lambda_m \tag{2}$$

$$L_d = \frac{\lambda_d - \lambda_m}{i_d} \tag{3}$$

$$L'_d = \frac{d\lambda_d}{di_d} \tag{4}$$

The methodology with differential inductance has been widely employed to detect changes in flux caused by demagnetization and eccentricity because its change with magnetic saturation is considerable compared to that of the inductance of the *d*-axis. A detailed explanation is provided by Hong *et al*. (2012), Haddad and Strangas (2016).

2.3 Simulation of flux linkage for d-axis inductance

To extract the *d*-axis inductance using Eq. (2), the magnetic flux needs to be determined via a simulation using ANSYS Maxwell 2D. The specifications of the PMSM used in this simulation and the experiment are listed in Table 1. A healthy motor and a faulty motor with demagnetization and eccentricity were modeled, and the flux density distribution was determined from the magnetostatic FE simulation, as shown in Fig. 3. Each fault was modeled with two-level severity. The air gap of the healthy PMSM is 0.5 mm. Eccentricity fault was emulated by changing the air gap by 0.15 mm and 0.30 mm for severity 1 and 2, respectively. PMs with degraded performances of 30% and 60%, with respect to that in healthy conditions, were

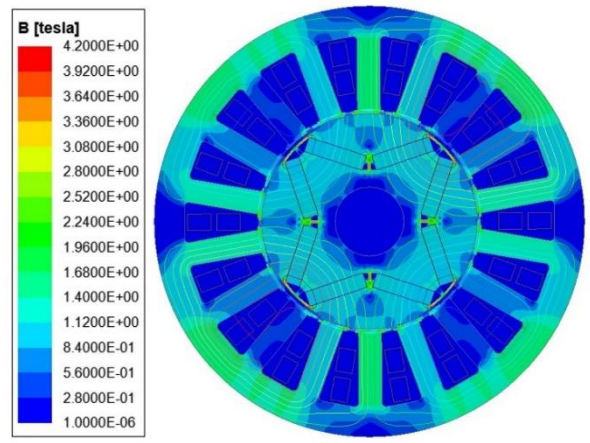

(a) Simulation result of healthy condition

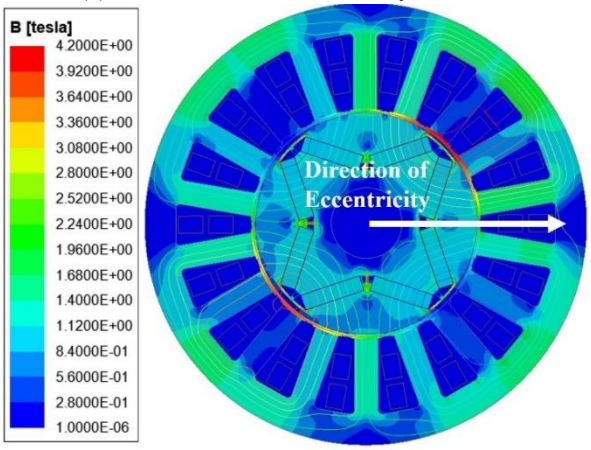

(b) Simulation result of eccentric condition

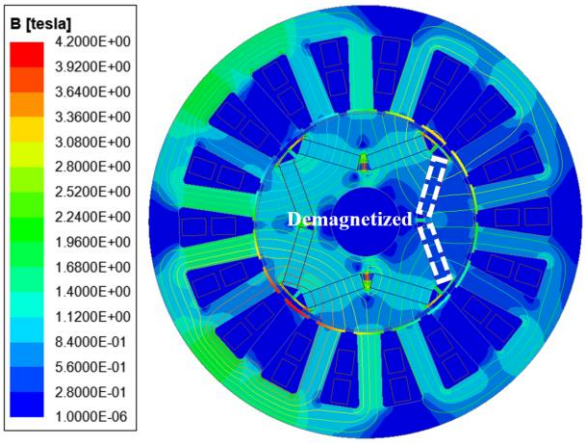

(c) Simulation result of demagnetized condition

Fig. 3 Magnetic flux density distribution of IPMSM

applied for severity 1 and 2, respectively.

The simulation results in Fig. 3 show the magnetic flux density of the motor in (a) healthy, (b) eccentric, (c) demagnetized conditions with no current flowing through the stator. In the case of the healthy condition, the magnetic flux density is uniform and symmetric based on the center of the motor. However, the flux density around the stator slightly increased on the side where the air gap was reduced (right side in Fig. 3(b)) caused by eccentricity. In contrast, the flux density on the side where the air gap was increased

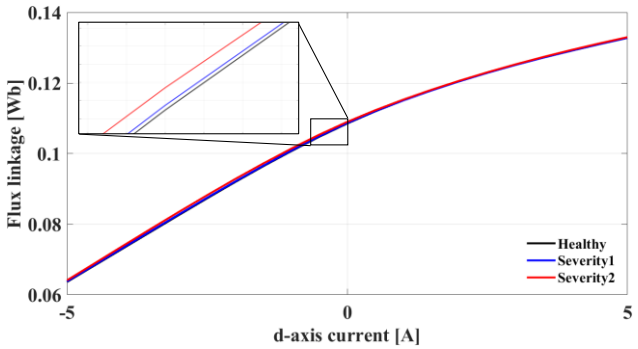

Fig. 4 Eccentricity PMSM *d*-axis flux linkage FEM results

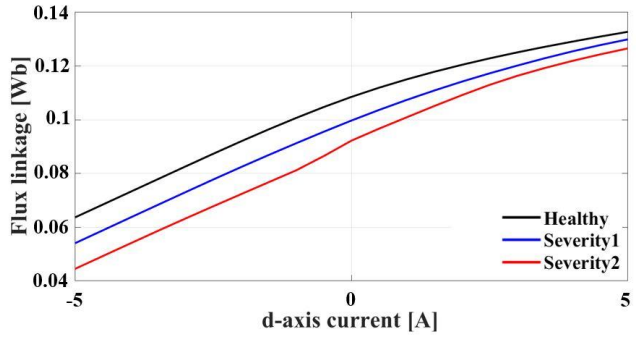

Fig. 5 Demagnetization PMSM *d*-axis flux linkage FEM results

(left side in the figure) slightly decreased. In the case of a motor with demagnetization, the flux density decreases around the stator where demagnetization occurs. Based on the result from the simulation, both the eccentricity and demagnetization cause changes in the flux linkage, resulting in changes in the inductance as explained with Eqs. (2)-(4). The *d*-axis magnetic flux calculated using 2D FEA simulation results of different motor conditions is shown in Figs. 4 and 5. Compared to that of the healthy motor, the flux density increases in the eccentric motor. On the contrary, it was confirmed that the magnetic flux decreases due to demagnetization. The *d*-axis magnetic flux also decreases as the severity of demagnetization increases. It means that more current in the *d*-axis is required to make the same amount of flux linkage.

3. Experimental study

3.1 Experiment setup

The detailed specifications of the PMSM used in this study are listed in Table 1. PMSM samples with eccentricity faults are emulated by shifting the shaft using a shim of 0.15 and 0.30 mm for severity 1 and severity 2, respectively. The shim is positioned as in Fig. 6(a). The Emulated fault is then verified with a computer tomography (CT) scan as shown in Fig. 6(c). In the case of demagnetization, two magnet bars corresponding to one rotor pole were divided into two pieces as shown in Fig. 6(b). After, one of the magnets was completely demagnetized by heating. The severity of demagnetization

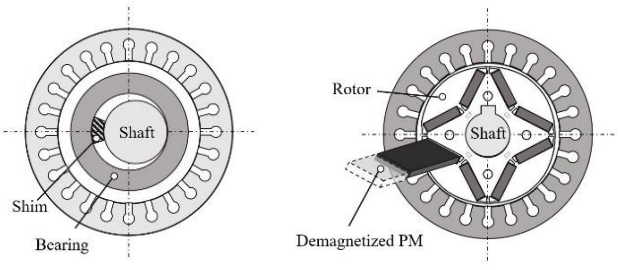

(a) Eccentricity (b) Demagnetization

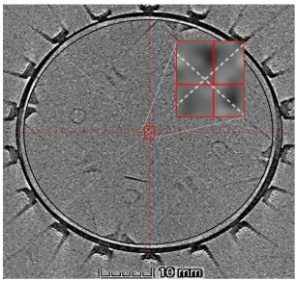

(c) Three-dimensional CT image confirming the deviation of rotor and stator center points in the eccentric motor

Fig. 6 IPMSM with artificially emulated eccentricity and demagnetization

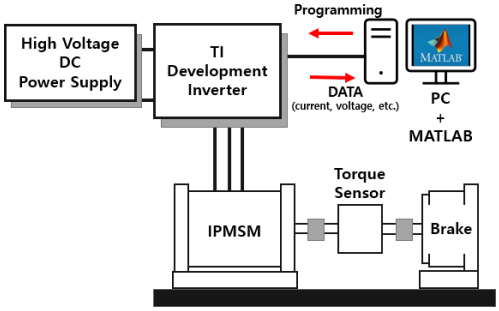

(a) Schematic representation of the experimental setup

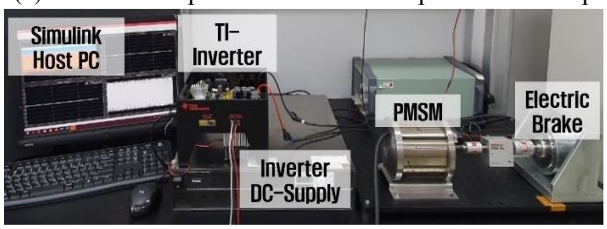

(b) Photograph of the experimental setup

Fig. 7 Experimental setup for IPMSM controlled by programmable TI inverter

was controlled by adjusting the ratio of the normal and completely demagnetized magnets.

The inverter was controlled through a TMS320F28335 Control-Card in a programmable development kit (TI, TMDSHVMTRPFCKIT). Commands to the digital signal processor (DSP) are issued through a serial peripheral interface using MATLAB Simulink. The data acquisition rate synchronized to the PWM frequency was set to 10 kHz.

Considering the rated current of 400-W PMSM used in this study, *d*-axis DC current from 0.5 to 2.5 A is applied in intervals of 0.5 A. Even though the saturation occurs after 5 A, the amplitude of the *d*-axis DC current was limited due

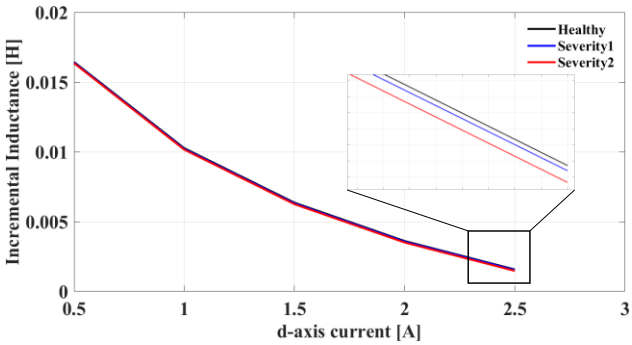

Fig. 8 Incremental inductance as a function of *d*-axis current for eccentricity

to the rated current of relatively small PMSM (0.4 kW) used in this study. An AC component of current with an amplitude of 0.1 A and frequency of 40 Hz was applied at each DC step considering the sensitivity of the incremental inductance. The amplitude and frequency of the AC current were optimized to increase the change in differential inductance.

3.2 Measuring inductance

As explained with Eqs. (2)-(4), both the inductance and incremental inductance can be determined by the magnetic flux density divided by the *d*-axis current. However, the magnetic flux can only be cacluated in simulation. The incremental inductance can be calculated using Eq. (5). The internal signal i_d (from 0.5 to 2.5 A) from programmable inverter was injected to the PMSM, and *d*-axis voltage command (v_d) was monitored. As i_d and v_d have a relation as shown in Eq. (5), L'_d can be calculated using the following equation

$$Z_{d,eq} = \frac{\vec{v}_d}{\vec{i}_d} = R_s + j\omega_e L'_d \tag{5}$$

$Z_{d,eq}$, and R_s, ω_e are the equivalent impedance of the *d*-axis, and reluctance, electrical excitation frequency, respectively.

3.3 Experimental result

The experimental results for the PMSM with eccentricity faults are shown in Fig. 8. Incremental inductance was experimentally determined based on Eq. (5) as described in the previous section. The results in Fig. 8 show clearly that the incremental inductance shifts to the lower left direction as the severity of eccentricity increases. The flux linkage of the d-axis increases as the eccentricity increases (the air gap decreases) as presented in the simulation result of Fig. 4 which indicates that magnetic circuit saturation occurs even with less current. It also means that the operation point is close to the knee point as shown in Fig. 2, where the slope of the inductance decreases resulting in a decrease in the incremental inductance. These results confirmed that the fault detection method presented in this paper can not only classify the existence but also differentiate the severity of the eccentric fault. Therefore, the decrease in the values the L'_d can be

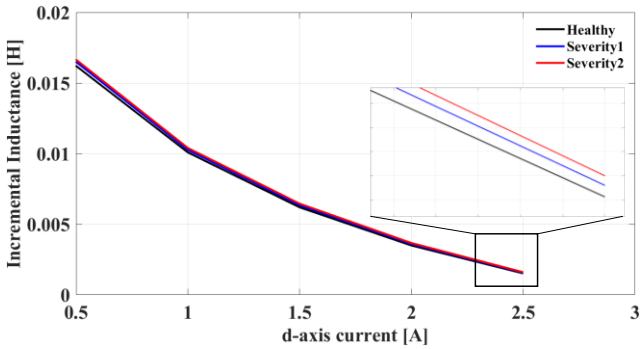

Fig. 9 Incremental inductance as a function of *d*-axis current for demagnetization

used as a fault indicator for eccentricity if it is monitored under identical excitation conditions.

In the case of demagnetization, the experimental results in Fig. 9 show that the incremental inductance shifts to the upper right as the severity of demagnetization increases. As presented in the simulation of Fig. 5, the flux linkage of the *d*-axis decreases as the severity of demagnetization increases. Contrary to the results shown with the eccentric motors, the operation point moves away from the knee point in Fig. 2. Therefore, the incremental inductance increases as the severity of demagnetization increases. Based on experimental results, it is confirmed that the programmable inverter, which is used for motor control, can be used to detect and classify the types of faults by implementing the algorithm. Therefore it is confirmed that additional sensors or systems were not required to detect and classify faults. Since fault diagnosis is carried out under standstill conditions, there is an advantage that the speed and load of the motor do not affect the performance of the diagnosis. In addition, it is also confirmed that this method can be applied to relatively small motors of the 0.4 kW class.

4. Conclusions

In this study, fault detection for eccentricity and demagnetization in PMSM was carried out based on the magnetic characteristics. The main concept is to monitor the voltage command signal and phase current of the PMSM under standstill conditions by injecting an optimized diagnostic signal. This method can detect the type of faults as well as their severity without the need for additional sensors and systems for detection.

FEA simulations were carried out to investigate the magnetic flux density of the IPMSM under healthy, as well as faulty conditions. It was confirmed that faults with eccentricity or demagnetization induced the change in magnetic flux density based on results from FEA as well as inductance based on the given equation. An experimental study for fault detection and classification, including their severity, was carried out with a 4-pole 0.4 kW PMSM controlled by a programmable TI inverter. Without any additional sensors or analyzers, all signals from the inverter were used to detect faults. In the case of an eccentric fault, the differential inductance decreased. In the case of a demagnetization fault, the differential inductance increased. Furthermore, differential inductance changes are amplified when the degree of failure becomes more severe. Therefore, it was confirmed that the proposed method could detect and classify faults and their severity.

Acknowledgments

This paper was written as part of Konkuk University's research support program for its faculty on sabbatical leave in 2020.

References

Bianchi, N. and Jahns, T.M. (2004), *Design, Analysis and Control of Interior PM Synchronous Machines*, CLEUP, Seattle, USA.

Chai, F., Li, Y., Liang, P. and Pei, Y. (2016), "Calculation of the maximum mechanical stress on the rotor of interior permanent-magnet synchronous motors", *IEEE Trans. Indus. Electron.*, **63**(6), 3420-3432. https://doi.org/10.1109/TIE.2016.2524410.

Espinosa, A.G., Rosero, J.A., Cusidó, J., Romeral, L. and Ortega, J.A. (2010), "Fault detection by means of hilbert–huang transform of the stator current in a PMSM with demagnetization", *IEEE Trans. Energy Convers.*, **25**(2). 312-318. https://doi.org/10.1109/TEC.2009.2037922.

Fasil, M., Antaloae, N., Mijatovic, N., Jensen, B.B. and Holboll, J. (2016), "Improved $ dq $-axes model of PMSM considering airgap flux harmonics and saturation", *IEEE Trans. Appl. Superconduct.*, **26**(4), 1-5. https://doi.org/10.1109/TASC.2016.2524021.

Haddad, R.Z. and Strangas, E.G. (2016), "On the accuracy of fault detection and separation in permanent magnet synchronous machines using MCSA/MVSA and LDA", *IEEE Trans. Energy Convers.*, **31**(3), 924-934. https://doi.org/10.1109/TEC.2016.2558183.

Hong, J., Park, S., Hyun, D., Kang, T.J., Lee, S.B., Kral, C. and Haumer, A. (2012), "Detection and classification of rotor demagnetization and eccentricity faults for PM synchronous motors", *IEEE Trans. Indus. Appl.*, **48**(3), 923-932. https://doi.org/10.1109/TIA.2012.2191253.

Kioumarsi, A., Moallem, M. and Fahimi, B. (2006), "Mitigation of torque ripple in interior permanent mmagnet motors by optimal shape design", *IEEE Trans. Magnet.*, **42**(11), 3706-3711. https://doi.org/10.1109/TMAG.2006.881093.

Le Roux, W., Harley, R.G. and Habetler, T.G. (2007), "Detecting rotor faults in low power permanent magnet synchronous Machines", *IEEE Trans. Power Electron.*, **22**(1), 322-328. https://doi.org/10.1109/TPEL.2006.886620.

Lee, S.B., Yang, J., Hong, J., Yoo, J.Y., Kim, B., Lee, K., ... & Nandi, S. (2011), "A new strategy for condition monitoring of adjustable speed induction machine drive systems", *IEEE Trans. Power Electron.*, **26**(2), 389-398. https://doi.org/10.1109/TPEL.2010.2062200.

Liu, X., Chen, H., Zhao, J. and Belahcen, A. (2016), "Research on the performances and parameters of interior PMSM used for electric vehicles", *IEEE Trans. Indus. Electron.*, **63**(6), 3533-3545. https://doi.org/10.1109/TIE.2016.2524415.

Nandi, S., Ahmed, S. and Toliyat, H.A. (2001), "Detection of rotor slot and other eccentricity related harmonics in a three-phase induction motor with different rotor cages", *IEEE Trans. Energy Convers.*, **16**(3), 253-260. https://doi.org/10.1109/60.937205.

Rajagopalan, S., Aller, J.M., Restrepo, J.A., Habetler, T.G. and Harley, R.G. (2006), "Detection of rotor faults in brushless DC

motors operating under nonstationary conditions", *IEEE Trans. Indus. Appl.*, **42**(6), 1464-1477. https://doi.org/10.1109/TIA.2006.882613.

Rosero, J., Cusido, J., Ortega, J.A., Garcia, A. and Romeral, L. (2007), "On-line condition monitoring technique for PMSM operated with eccentricity", *2007 IEEE International Symposium on Diagnostics for Electric Machines, Power Electronics and Drives*, September.

Soong, W.L. and Ertugrul, N. (2002), "Field-weakening performance of interior permanent-magnet motors", *IEEE Trans. Indus. Appl.*, **38**(5), 1251-1258. https://doi.org/10.1109/TIA.2002.803013.

Wang, S. and Li, H. (2021), "Analysis of electromagnetic vibration of permanent magnet synchronous motor under static and dynamic eccentricity fault", *2021 6th International Conference on Control and Robotics Engineering (ICCRE)*, April.

Wardach, M., Paplicki, P. and Palka, R. (2018), "A hybrid excited machine with flux barriers and magnetic bridges", *Energies*, **11**(3), 676. https://doi.org/10.3390/en11030676.

Wu, L., Huang, X., Habetler, T.G. and Harley, R.G. (2007), "Eliminating load oscillation effects for rotor eccentricity detection in closed-loop drive-connected induction motors", *IEEE Trans. Power Electron.*, **22**(4), 1543-1551. https://doi.org/10.1109/TPEL.2007.900542.